Some Effects of Anisotropy on Planar Antiresonant Reflecting Optical Waveguides

Bishwabandhu Ray and George W. Hanson

Abstract— **In this paper, propagation characteristics of some planar antiresonant reflecting optical waveguides (ARROW's) comprised of anisotropic media are studied using an integral equation approach. The integral equation method is rigorous and general, with the added advantage that multiple layers of crystalline material with arbitrary anisotropy can be accommodated in a straightforward manner. The integral equation method is applied to study basic propagation characteristics of the ARROW structure where one or more dielectric layers are allowed to be anisotropic. Practically, the presence of anisotropy may be unintentional, due to material fabrication or processing techniques, or it may be intentionally utilized to allow integration of anisotropy-based devices and waveguiding structures on a single semiconducting substrate. Propagation characteristics and field distributions are shown for a uniaxially anisotropic ARROW where the material's optic axis is rotated in each of the three principal geometrical planes of the structure. It is found that even moderately large levels of anisotropy do not significantly affect the propagation characteristics of the ARROW if either the optic axis of the material is aligned with one of the geometrical axes of the waveguide, or if the optic axis is rotated in the equatorial plane. In these cases, pure TE_0 modes can propagate, resulting in a low-loss structure. In the event of misalignment between the geometrical axes and the material's optic axis in the transverse or polar planes, the influence of even small levels of anisotropy is quite pronounced. In this case, pure TE_0 modes do not exist, and attenuation loss increases significantly due to the hybrid nature of the fundamental mode.**

I. Introduction

OPTICAL waveguides integrated on semiconductor substrates allow for the possibility of integrating active and passive optical devices, and for incorporating electrical and optical circuits on a single substrate. Due to the large refractive index of semiconducting materials, it is difficult to confine light to a conventional optical waveguide core, resulting in large propagation loss due to the lack of total internal reflection at the waveguide/semiconductor interface. One method of obtaining a low-loss structure is to isolate the waveguide core from the semiconductor with a thick layer of transparent material. This method may not be desirable from a fabrication or utilization standpoint. An alternative waveguiding structure, the antiresonant reflecting optical waveguide (ARROW) has been developed to provide a low-loss optical waveguide on a semiconducting substrate [1]. The ARROW structure posses several desirable features [2]. It has a large waveguiding core to facilitate efficient coupling to optical fibers, while providing essentially single-mode propagation by the loss discrimination of higher order modes. It is also relatively insensitive to the thickness and refractive index of its constituent layers, as long as the antiresonant condition is approximately satisfied. Basic propagation characteristics and applications of ARROW structures have been presented in [1]–[9].

In all of the previous investigations, the material layers have been isotropic. There are several reasons for studying the effect of anisotropy on ARROW characteristics. ARROW-type waveguides have recently been utilized in structures that are more complicated than those previously considered, including acousto-optic applications [10] and in structures with deposited metal strips [11] to enhance polarization discrimination. As the range of materials and geometries that utilize ARROW characteristics increases, it is important to ascertain the effect of anisotropy, either intentional or unintentional, on propagation characteristics. For instance, anisotropy caused by material processing or fabrication techniques, although unintended, may be present in an integrated optical circuit. Examples include residual strain in grown heterostructure layers, strain caused by metallic strip loading or in three-dimensional channel guides, leading to birefringence due to the photoelastic effect, and electro-optic induced birefringence in crystallin materials due to stray electric fields [12].

It is also of interest to study anisotropic ARROW structures since many anisotropic materials have desirable qualities in the optical regime. These materials often possess low-loss and large electro-optic and photoelastic effects, which form the basis of many applications. The incorporation of materials with naturally occurring or intentionally induced anisotropy in hybrid or monolithic integrated optical circuits leads to greater flexibility and functionality. For instance, a hybrid integrated optical circuit is described in [13], utilizing silicon and $LiNbO_3$. It may be possible to construct new or more efficient anisotropy-based devices on semiconductor substrates in an ARROW configuration, using more complicated materials.

In this paper, a general numerical method is developed to study inhomogeneous anisotropic waveguides, with specific application to ARROW structures. Although analytical methods exist to study planar anisotropic waveguides (see [14], for instance), the method presented here is relatively simple to implement, and anisotropic media with graded-index or stepwise-constant inhomogeneities can be accommodated easily. The method follows from a polarization-type integral equation (IE) using the relatively simple Green's function for an isotropic homogeneous half-space. The IE is converted into a homogeneous matrix equation, and a root search is performed

Manuscript received May 15, 1995; revised Ocotber 13, 1995.

The authors are with the Department of Electrical Engineering and Computer Science, University of Wisconsin—Milwaukee, Milwaukee, WI 53201 USA.

Publisher Item Identifier S 0733-8724(96)01424-7.

to determine the value of the propagation constant which forces the matrix determinate to vanish. Similar IE's have been used to study three dimensional waveguiding geometries, including isotropic rectangular step-index, graded-index and rib waveguides [15]–[17], and anisotropic channel waveguides [18], [19]. For three-dimensional waveguides, the matrix entries need to be determined by numerically performing spectral inverse Fourier transform integrals. An advantage of applying this technique to planar two-dimensional structures as described here is that the matrix entries are determined analytically, so that relativity complicated structures can be efficiently analyzed. Although applied to the source-free problem here, the IE method also easily accounts for forced problems, and has been used to study excitation of guided and radiation modes of conventional three-layer, asymmetric isotropic planar waveguides [20], [21], and to determine Green's function components for multilayered anisotropic structures [22].

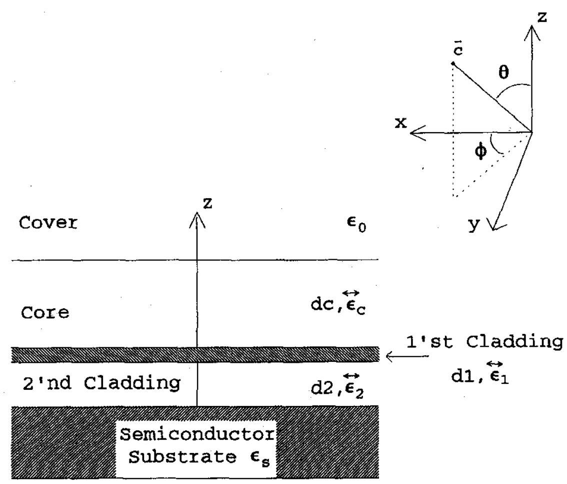

Fig. 1. Anisotropic ARROW waveguiding structure.

II. THEORY

Consider the planar ARROW waveguiding structure shown in Fig. 1. An isotropic substrate material with $\epsilon = \epsilon_s$ and an isotropic cover layer having $\epsilon = \epsilon_0$ occupy $z < 0$ and $z > D$, respectively, where $D = d_1 + d_2 + d_c$. A general inhomogeneous anisotropic region occupies the space between cover and substrate. In the absence of the anisotropic region, the electric field in the region $z > 0$ due to a polarization source ($\vec{p} = \vec{J}/j\omega$) is given by [23]

$$\vec{e}(k_y, z) = \int_z \overleftrightarrow{g}^e (k_y, z \mid z') \cdot \vec{p}(k_y, z') dz' \tag{1}$$

where various components of the Green's dyadic are given in the Appendix. The above expression is for the field in the two-dimensional Fourier transform domain,

$$\vec{e}(k_x, k_y, z) = \iint_{-\infty}^{\infty} \vec{E}(x, y, z) e^{-j(k_x x + k_y y)} dx dy$$
$$\vec{E}(x, y, z) = \frac{1}{(2\pi)^2} \iint_{-\infty}^{\infty} \vec{e}(k_x, k_y, z) e^{j(k_x x + k_y y)} dk_x dk_y \tag{2}$$

where the dependence on the transverse wavenumber k_x has been suppressed. Since the structures of interest here are invariant in x, with waves propagating in the y-direction as $e^{-jk_y y}$, we set $k_x = 0$. To account for an anisotropic region as shown in Fig. 1, consider Ampere's law for the anisotropic region of interest, $\nabla \times \vec{h} = j\omega\vec{p}^i + j\omega\overleftrightarrow{\epsilon}(z) \cdot \vec{e}$ where $\vec{p}^i$ represents an impressed polarization. Adding and subtracting the term $j\omega\epsilon_0\vec{e}$ leads to $\nabla \times \vec{h} = j\omega(\vec{p}^i + \vec{p}_{\text{eq}}) + j\omega\epsilon_0\vec{e}$ where $\vec{p}_{\text{eq}} = [\overleftrightarrow{\epsilon}(z) - \epsilon_0\overleftrightarrow{I}] \cdot \vec{e}$. With the appropriate identification of the equivalent polarization current, the inhomogeneous anisotropic region without polarization currents can be replaced with a homogeneous free space region containing the unknown polarization currents. An integral equation can be formed by forcing the total electric field in the free-space region (formally occupied by the anisotropic media) to equal the impressed field plus the scattered field maintained by the equivalent polarization current,

$$\vec{e}(k_y, z) - \int_z \overleftrightarrow{g}^e (k_y, z \mid z') \cdot [\overleftrightarrow{\epsilon}(z') - \epsilon_0 \overleftrightarrow{I}] \cdot \vec{e}(k_y, z') dz'$$
$$= \vec{e}^i(k_y, z) \cdots \forall \quad 0 < z < D. \tag{3}$$

Since we are interested in natural surface-wave modes of the structure, the impressed field term, $\vec{e}^i(k_y, z)$, is set to zero. The value of the propagation constant k_y which satisfies (3) is the desired surface-wave propagation constant.

The above integral equation is solved using a pulse-function, method of moments (MoM)/Galerkin procedure [24]. The unknown field over the range $0 \leq z \leq D$ is expanded in a set of pulse functions as

$$\vec{e}(k_y, z) = \sum_{\beta = x, y, z} \sum_{n=1}^{N} \hat{\beta} a_n^\beta(k_y) p_n(z) \tag{4}$$

where

$$p_n(z) = \begin{cases} 1 & z_n - \frac{w_n}{2} \leq z \leq z_n + \frac{w_n}{2} \\ 0 & \text{otherwise} \end{cases},$$

w_n is the width of the nth pulse, and a_n^β is an unknown amplitude. Testing with $\int_z dz p_{ng}(z)\hat{\alpha}$, for $\hat{\alpha} = \hat{x}, \hat{y}, \hat{z}$ results in a $(3N) \times (3N)$ matrix system, $[Z(k_y)][a] = 0$. Waveguide modes are obtained by a root search for the complex value of the propagation constant k_y which results in $\text{DET}[Z(k_y)] = 0$. Field profiles are obtained from the nullspace of the matrix $[Z(k_y)]$ evaluated at the resonant wavenumber.

Extensive numerical tests were performed to validate the above theory [25]. Propagation constants and field profiles were compared to results obtained using the standard transcendental eigenvalue equation and analytical field expressions for the first several TE and TM modes of a simple three-layer symmetric and asymmetric slab waveguide [26]. Forward and backward propagation constants for an asymmetric slab magnetoopic waveguide were compared to results in [27]. Results for a uniaxial symmetric slab waveguide were compared to those in [28] where propagation constants were determined as a function of rotation of the material's optic axis in the transverse (z-x), equatorial (z-y), and polar (x-y) planes. Results were also compared to those in [2] for an isotropic ARROW structure. In all cases results based upon the above theory were seen to agree closely with previously published results.

III. Application to ARROW

The integral equation method developed above was applied to the ARROW structure shown in Fig. 1. Geometrical properties and electrical characteristics were chosen similar to values listed in [2]–[5] in order to provide the most direct comparison to the familiar isotropic structure. Various anisotropy ratios (AR $= n_o/n_e$, with n_o, n_e the ordinary and extraordinary refractive indiexes, respectively) were chosen to demonstrate the effect on propagation characteristics. In the following figures, the isotropic substrate was assumed to be silicon with $n_s = 3.85$, and the isotropic cover layer was air. The wavelength was chosen to be 0.633 μm, with structural parameters dc = 4 μm, d2 = 2 μm, and d1 = 0.088 62 μm. The relative permittivity of layer i had the general form

$$[\epsilon_i] = R_i(\theta,\phi)\begin{bmatrix} n_{o,i}^2 & 0 & 0 \\ 0 & n_{o,i}^2 & 0 \\ 0 & 0 & n_{e,i}^2 \end{bmatrix} R_i^T(\theta,\phi)$$

where $R(\theta,\phi)$ is an orthogonal rotation matrix which rotates the crystal coordinate system relative to the waveguiding coordinate system. The matrix R^T is the transpose of matrix R, and (θ,ϕ) are the usual spherical angles which rotate the optic axis of layer i, as shown in Fig. 1. Waves were assumed to propagate as $e^{-jk_y y}$ where k_y satisfies the homogeneous form of (3). In all cases the extraordinary refractive indexes were $n_{e,2} = n_{e,c} = 1.46$, $n_{e,1} = 2.3$, and the values of n_o, θ, ϕ varied for each layer. These values, along with the thicknesses listed above, correspond to an ARROW structure operated at first antiresonance in the isotropic limit, $n_o = n_e$ [2]–[5].

Although results are not shown here, it was found that when the core and cladding layers of the ARROW are anisotropic with the optic axis aligned with one of the geometrical axes ($\theta = \phi = 0°$ for instance), propagation characteristics are approximately the same as for isotropic media. Attenuation did not increase even for relatively large levels of anisotropy, e.g., AR = 1.2. This is because pure TE modes can exist for these structures, and the electric field $\vec{e} = \hat{x}e_x$ is sensitive to the refractive index in the x-direction only. The antiresonance effect for TE modes seems to occur as in the isotropic case. This indicates, assuming no misalignment between the crystal and waveguiding coordinate systems, that anisotropic materials may be utilized in ARROW configurations where propagation characteristics can be controlled by the x-component of the refractive index.

In the following, propagation characteristics of low-order TE, TM, and hybrid modes are studied for a uniaxially anisotropic ARROW where the optic axis is rotated in the three principal geometrical planes. Field distributions are shown to illustrate the various mode transformations which occur under optic axis rotation, and to aid in interpreting the plots of

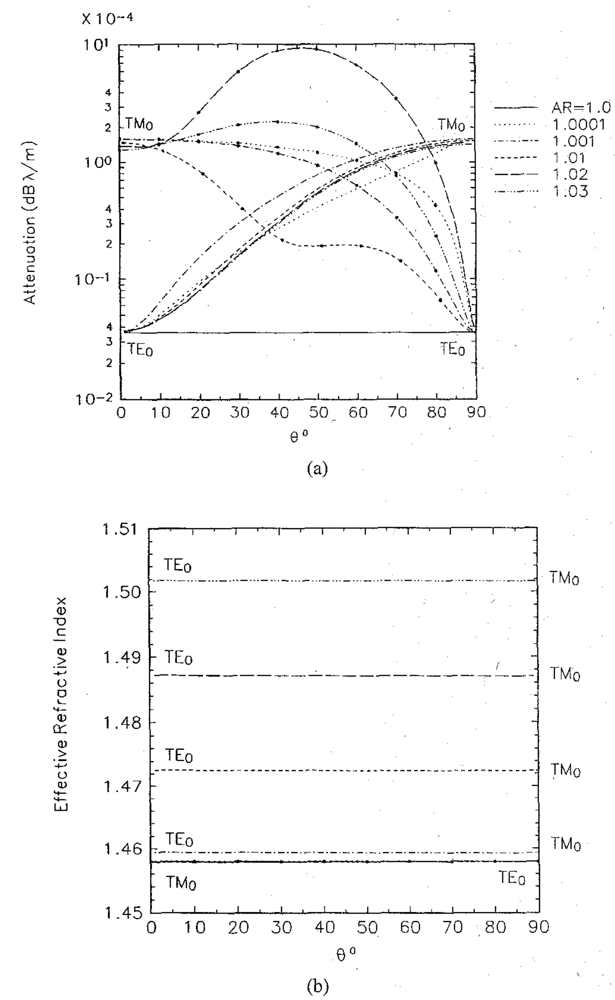

Fig. 2. Attenuation (a) and effective refractive index (b) versus orientation of optic axis in transverse (z–x) plane for various values of AR. Mode evolution $TE_0 \rightarrow TM_0$ (no dots) and $TM_0 \rightarrow TE_0$ (dots) occurs with increasing angle θ, $\phi = 0°$.

propagation characteristics. Although the method presented is general, the simple case of all layers being anisotropic with the same value of AR is studied here. Practically, it is the presence of anisotropy in the core region which provides the strongest influence over propagation characteristics. It is found that, unlike in the preceding case where the optic axis aligns with one of the geometrical axes, attenuation is significantly increased when misalignment occurs in the transverse and polar planes due to the hybrid nature of the modes. In the equatorial plane, pure TE modes can exist, and low loss propagation occurs as in the isotropic ARROW.

Fig. 2 shows the effect on propagation characteristics of rotating the optic axis in the transverse (z-x) plane (θ varies, $\phi = 0°$) for various anisotropy ratios. Attenuation is shown in Fig. 2(a), and effective refractive index is shown in Fig. 2(b). In the attenuation plots, the set of curves increasing (decreasing) from left to right represent the evolution of modes $TE_0 \rightarrow TM_0$ $TM_0 \rightarrow TE_0$ as the optic axis is rotated in the transverse plane from $\theta = 0°$ to $\theta = 90°$. This mode

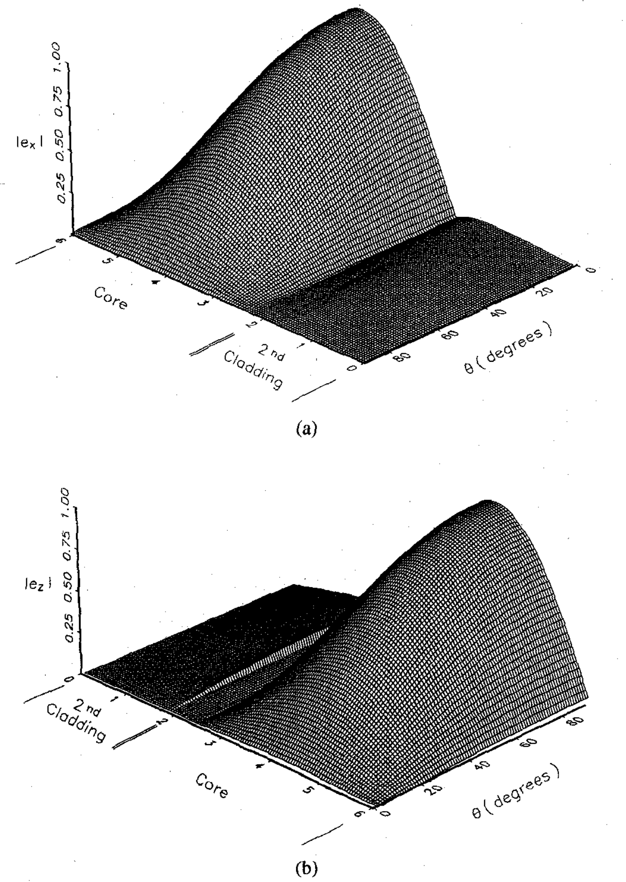

Fig. 3. Field component e_x (a) and e_z (b) versus position and rotation angle in the traverse plane for $TE_0 \rightarrow TM_0$ mode evolution as $\theta = 0° \rightarrow 90°$, $\phi = 0°$, AR=1.03.

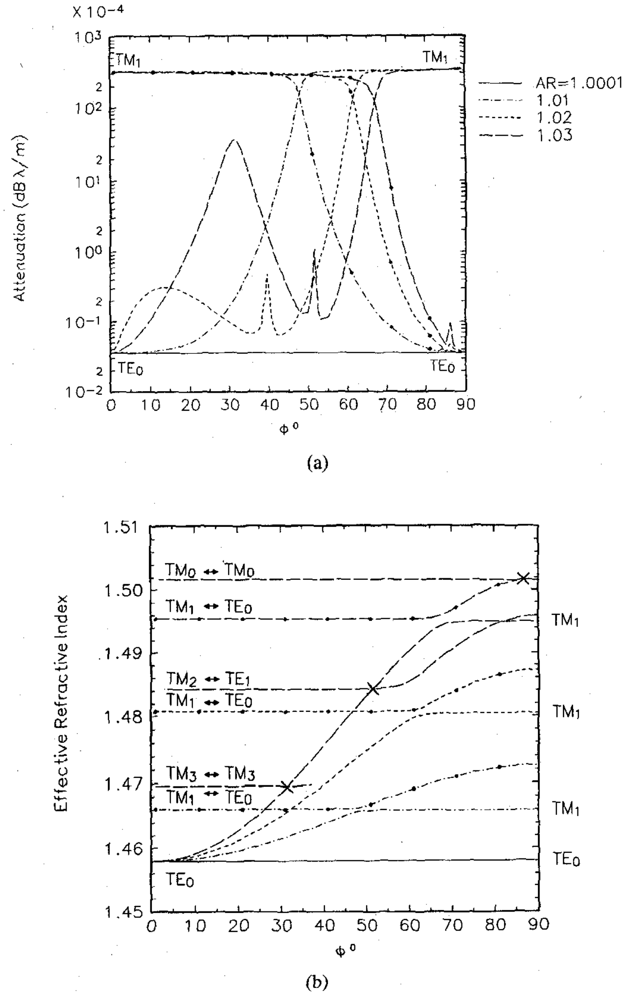

Fig. 4. Attenuation (a) and effective refractive index (b) versus orientation of optic axis in polar (x–y) plane for various values of AR. Mode evolution $TE_0 \rightarrow TM_1$ (no dots) and $TM_1 \rightarrow TE_0$ (dots) occurs with increasing angle ϕ, $\theta = 90°$.

transformation, with the corresponding flat dispersion behavior shown in Fig. 2(b), is identical to that observed in [28] for a single uniaxial slab under rotation in the transverse plane. It is seen that attenuation significantly increases for $\theta \neq 0°$, 90°. This is because a pure TE_0 mode cannot exist, and the resulting hybrid-mode field is not confined to the core by the antiresonance effect. As the TE_0 mode evolves into the TM_0 mode, the attenuation tends toward that of the TM_0 mode in an isotropic ARROW. It should be noted that very small levels of anisotropy lead to TE $\rightarrow$ TM mode evolution with a corresponding increase in attenuation.

The effective refractive index, $\mathrm{Re}\{k_y\}/k_0$ where $k_0 = 2\pi/\lambda_0$, for the ($0° \rightarrow 90°$) $TE_0 \rightarrow TM_0$ cases are constant as a function of θ, but depend on the x-component of core refractive index $n_{x,c} = 1.46$ AR at $\theta = 0°$, in agreement with [28]. The $0° \rightarrow 90°$, $TM_0 \rightarrow TE_0$ cases (or equivalently $90° \rightarrow 0°$, $TE_0 \rightarrow TM_0$ cases) overlap each other, since for $\theta = 90°$ $n_{x,c} = 1.46$, independent of AR value.

In order to help explain the above attenuation and dispersion behavior, three dimensional plots of the electric field versus position in the waveguide and rotation angle are shown in Fig. 3. Fig. 3(a) and (b) show the field components e_x, e_z as the optic axis is rotated from the z-axis to the x-axis ($\theta = 0° \rightarrow 90°$, $\phi = 0°$) for AR = 1.03. It can be seen that as the rotation angle increases, the e_x component decreases while the e_z component increases, and the mode undergoes a smooth transition $TE_0 \rightarrow TM_0$. Similar behavior was observed for the mode evolution $TM_0 \rightarrow TE_0$.

The effect of rotating the optic axis in the polar (x–y) plane ($\theta = 90°, \phi$ varies) is shown in Fig. 4. In the attenuation plots of Fig. 4(a), the set of curves increasing (decreasing) from left to right represent the evolution of modes $TE_0 \rightarrow TM_1 (TM_1 \rightarrow TE_0)$ as the optic axis is rotated in the polar plane from $\phi = 0°$ to $\phi = 90°$. This mode transformation, and the corresponding dispersion behavior shown in Fig. 4(b), is similar to that observed in [28] for a single uniaxial slab under rotation in the polar plane. It is seen that attenuation significantly increases if the optic axis is not aligned with one of the waveguiding axes in this plane. As for rotations in the transverse plane, a pure TE_0 mode cannot exist under rotations in the polar plane, resulting in a hybrid TE–TM mode with larger attenuation. The sharp spikes in the attenuation plot are due to the intersection of the effective refractive index

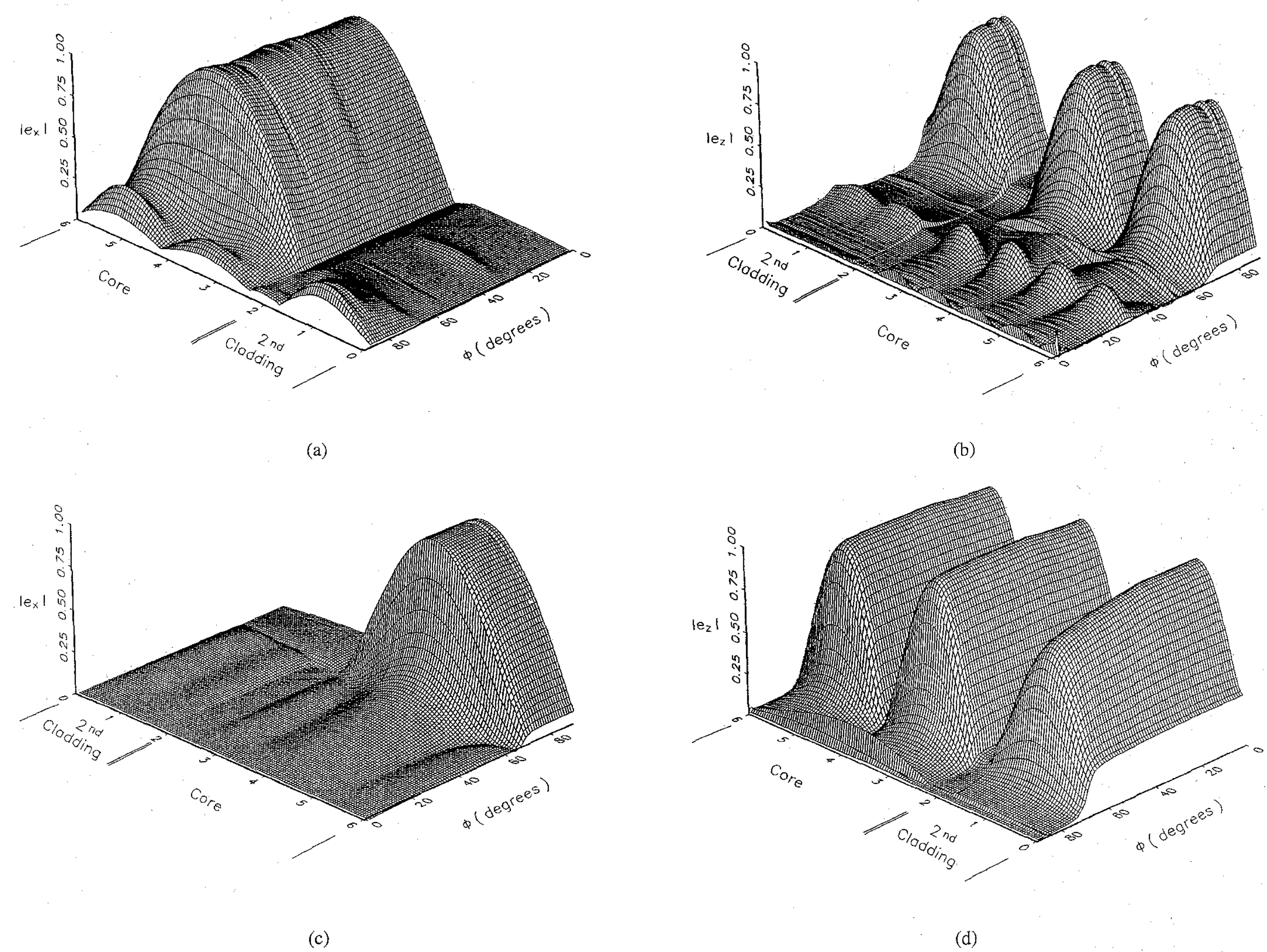

Fig. 5. Field component e_x (a) and e_z (b) versus position and rotation angle in the polar plane for $TE_0 \rightarrow TM_0$ mode evolution as $\phi = 0° \rightarrow 90°$, $\theta = 0°$, AR = 1.03. Field component e_z (c) and e_x (d) versus position and rotation angle in the polar plane for $TM_1 \rightarrow TE_0$ mode evolution as $\phi = 0° \rightarrow 90°$, $\theta = 0°$, AR = 1.03.

curve for a particular modal evolution with another hybrid mode. At these points a degeneracy exists where the real part of the propagation constants are equal. These crossings occur primarily for rotations in the polar plane, but also in the transverse plane for some higher order modes. The dispersion curves in [28] clearly show this where modes up to TE_4/TM_4 are considered. The effective refractive index curves shown in Fig. 4(b) for the $TE_0 \leftrightarrow TM_1$ mode evolutions show similar behavior to the simple single-slab uniaxial case in [28]. The points of mode degeneracy which lead to the spikes in the attenuation curves for AR = 1.03 can be clearly seen. The peak at $\phi \approx 32°$ in the $TE_0 \rightarrow TM_1$ attenuation curve is due to the refractive index curve crossing the $TM_3 \rightarrow TM_3$ modal evolution, a portion of which is shown in the figure. The peak at $\phi \approx 51°$ in attenuation is due to the refractive index curve crossing the $TM_2 \rightarrow TE_1$ modal evolution. The peak at $\phi \approx 86°$ in the $TM_1 \rightarrow TE_0$ attenuation curve is due to the refractive index curve crossing the $TM_0 \rightarrow TM_0$ modal evolution. These three points are marked with an X in Fig. 4(b). Similar behavior was found for AR = 1.02, but the mode intersections are not shown here.

Three-dimensional field plots are shown in Fig. 5 for the modal evolution $TE_0 \rightarrow TM_1$ and $TM_1 \rightarrow TE_0$. It can be seen that peaks in attenuation correspond to increases in the cladding field at certain angles. The spike at $\phi \approx 32°$ in the $TE_0 \rightarrow TM_1$ attenuation curve described above, due to the mode crossing the $TM_3 \rightarrow TM_3$ modal evolution, can be seen in Fig. 5(b). The degeneracy at $\phi \approx 51°$ due to the crossing with the $TM_2 \rightarrow TE_1$ mode can also be seen in Fig. 5(b) as a disturbance in the field pattern. The $TM_2 \rightarrow TE_1$ mode crosses the $TE_0 \leftrightarrow TM_1$ mode of interest a second time at $\phi \approx 83°$, which can be seen in Fig. 5(a). The $TM_1 \rightarrow TE_0$ attenuation curve spike at $\phi \approx 86°$ due to intersection with the $TM_0 \rightarrow TM_0$ mode is clearly seen in Fig. 5(d).

It is seen from the propagation characteristics and field behavior that the evolution of the TE_0 mode to a TM mode is very different in the transverse and polar planes, and is asymmetric for rotations in different directions in the same plane.

Finally, the effect of rotation in the equatorial (z–y) or decoupled plane is shown in Fig. 6. At all values of rotation in this plane, pure TE_0 may exist, and the attenuation curves

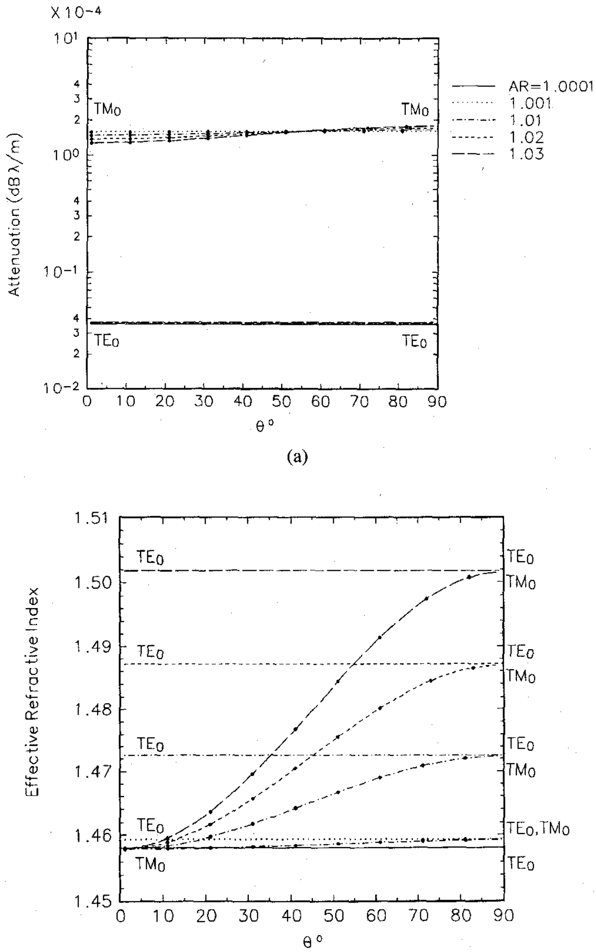

Fig. 6. Attenuation (a) and effective refractive index (b) versus orientation of optic axis in the equatorial z–y plane for various values of AR. Pure TE_0 (no dots) and TM_1 (dots) modes exist for all angles of rotation θ, $\phi = 90o$.

are constant with angular rotation. For completeness, TM_0 modes are also shown, for which the dispersive behavior of the effective refractive index is in agreement with the single-slab uniaxial case [28].

The above figures are intended to show modal evolution as a function of optic axis rotation. The excitation problem is not considered, such as mode coupling from an input waveguide to the ARROW structure. Since the ARROW waveguide only has low loss for the TE_0 mode, feeding waveguides would present a TE-polarized mode. This mode would couple most strongly to the TE_0 mode if the optic axis is oriented such that it can exist. In the event of a hybrid mode, the input excitation would probably couple most strongly to the mode with the largest TE component, although this was not studied here.

In summary, when the crystal and waveguiding axes coincide, even moderately large levels of anisotropy do not significantly alter the propagation characteristics of the anisotropic ARROW waveguide from its isotropic counterpart, since pure TE_0 modes may exist. This is also true for optic axis rotations in the equatorial plane. In the event that the optic axis is rotated about the geometrical axes in the transverse or polar planes, or some combination of the two, even small levels of anisotropy strongly affect the attenuation constant due to the hybrid nature of the resulting modes.

IV. Conclusion

The effect of anisotropy on the propagation characteristics of planar antiresonant reflecting optical waveguides (ARROW's) has been studied using an integral equation (IE) approach. An IE formulation has been developed which is applicable to generally inhomogeneous anisotropic media, with specific application to the stratified ARROW structure where one or more dielectric layers are allowed to be anisotropic. It was found that even moderately large levels of anisotropy do not significantly affect the propagation characteristics of the ARROW if the optic axis of the material is aligned with one of the geometrical axes of the waveguiding structure, or for optic axis rotations in the equatorial plane. This indicates that anisotropic media may be incorporated into ARROW-type configurations on semiconducting substrates, allowing for greater flexibility and functionality. In the event of optic axis misalignment in the transverse or polar planes, the influence of anisotropy is quite pronounced. In this case, attenuation loss increases due to the hybrid (TE–TM) nature of the fundamental mode. This effect may be less pronounced for rotation in the transverse plane ($TE_0 \rightarrow TM_0$) for the ARROW-B configuration, since that geometry has reduced TM_0 mode loss [2].

Appendix

The Green's dyadic for an isotropic two-layer geometry in the two-dimensional Fourier transform plane (k_x, k_y) for any $(z, z' \geq 0)$ is given as

$$\overleftrightarrow{g}^e (k_x, k_y, z \mid z') = [\overleftrightarrow{g} (k_x, k_y, z \mid z') - \hat{z}\hat{z}\delta(z - z')]/\epsilon_c$$

with components

$$\begin{aligned}
g_{xx} &= \{(k_c^2 - k_x^2)[e^{-p_c|z-z'|} + R_t e^{-p_c(z+z')}] \\
&\quad + k_x^2 p_c C e^{-p_c(z+z')}\}/2p_c \\
g_{xy} &= \{k_x k_y (p_c C - R_t) e^{-p_c(z+z')} - k_x k_y e^{-p_c|z-z'|}\}/2p_c \\
g_{xz} &= \{-jk_x p_c [\operatorname{sgn}(z - z') e^{-p_c|z-z'|} \\
&\quad + R_n e^{-p_c(z+z')}]\}/2p_c \\
g_{yx} &= g_{xy} \\
g_{yy} &= \{(k_c^2 - k_y^2)[e^{-p_c|z-z'|} + R_t e^{-p_c(z+z')}] \\
&\quad + k_y^2 p_c C e^{-p_c(z+z')}\}/2p_c \\
g_{yz} &= \{-jk_y p_c [\operatorname{sgn}(z - z') e^{-p_c|z-z'|} \\
&\quad + R_n e^{-p_c(z+z')}]\}/2p_c \\
g_{zx} &= \{(k_c^2 + p_c^2) jk_x C e^{-p_c(z+z')} - jk_x p_c \\
&\quad \times [\operatorname{sgn}(z - z') e^{-p_c|z-z'|} + R_t e^{-p_c(z+z')}]\}/2p_c \\
g_{zy} &= \{(k_c^2 + p_c^2) jk_y C e^{-p_c(z+z')} - jk_y p_c \\
&\quad \times [\operatorname{sgn}(z - z') e^{-p_c|z-z'|} + R_t e^{-p_c(z+z')}]\}/2p_c \\
g_{zz} &= \{(k_c^2 + p_c^2)[e^{-p_c|z-z'|} + R_n e^{-p_c(z+z')}]\}/2p_c
\end{aligned}$$

where

$$R_t = \frac{p_c - p_s}{p_c + p_s}, R_n = \frac{N^2 p_c - p_s}{N^2 p_c + p_s}, C = \frac{2(N^2 - 1)p_c}{(p_c + p_s)(N^2 p_c + p_s)}$$

with $p_{c,s} = \sqrt{k_x^2 + k_y^2 - k_{c,s}^2}$, $N = n_s/n_c$, $n_{s,c} = \sqrt{\mu_0 \epsilon_{s,c}}$,

$$k_{c,s} = n_{c,s}k_0, \text{ and } \operatorname{sgn}(z) = \begin{cases} 1 & z > 0 \\ -1 & z < 0 \\ 0 & z = 0 \end{cases}.$$

REFERENCES

[1] M. A. Duguay, Y. Kokubun, T. L. Koch, and L. Pfeiffer, "Antiresonant reflecting optical waveguides in SiO_2-Si multilayer structures," *Appl. Phys. Lett.*, vol. 49, pp. 13–15, July 1986.

[2] T. Baba and Y. Kokubun, "Dispersion and radiation loss characteristics of antiresonant reflecting optical waveguides-numerical results and analytical expressions," *IEEE J. Quantum Electron.*, vol. 28, pp. 1689–1700, July 1992.

[3] T. Baba, Y. Kokubun, T. Sakaki, and K. Iga, "Loss reduction of an ARROW waveguide in shorter wavelength and its stack configuration," *J. Lightwave Tech.*, vol. 6, pp. 1440–1444, Sept. 1988.

[4] T. Baba and Y. Kokubun, "Scattering loss of antiresonant reflecting optical waveguides," *J. Lightwave Tech.*, vol. 9, pp. 590–597, May 1991.

[5] ——, "High efficiency light coupling from antiresonant reflecting optical waveguide to integrated photodetector using an antireflecting layer," *Appl. Opt.*, vol. 29, pp. 2781–2791, June 1990.

[6] T. Baba, Y. Kokubun, and H. Watanabe, "Monolithic integration of an ARROW-type demultiplexer and photodetector in the shorter wavelength region," *J. Lightwave Tech.*, vol. 8, pp. 99–104, Jan. 1990.

[7] M. Cantin, C. Carignan, R. Cote, M. A. Duguay, R. Larose, P. LeBel, and F. Quellette, "Remotely switched hollow-core antiresonant reflecting optical waveguide," *Opt. Lett.*, vol. 16, pp. 1738–1740, Nov. 1991.

[8] J. L. Archambault, R. J. Black, S. Lacroix, and J. Bures, "Loss calculations for antiresonant waveguides," *J. Lightwave Tech.*, vol. 11, pp. 416–423, Mar. 1993.

[9] Z. M. Mao and W. P. Huang, "An ARROW optical wavelength filter: Design and analysis," *J. Lightwave Tech.*, vol. 11, pp. 1183–1188, July 1993.

[10] E. S. Tony and S. K. Chaudhuri, "An ARROW directional coupler acousto-optic filter," in *IEEE AP-S Int. Symp. URSI Radio Sci. Meeting*, Seattle, WA, June 1993, Digest, pp. 1362–1365.

[11] U. Trutschel, M. Cronin-Golomb, G. Fogarty, F. Lederer, and M. Abraham, "Analysis of metal-clad antiresonant reflecting optical waveguide for polarizer applications," *IEEE Photon. Technol. Lett.*, vol. 5, pp. 336–339, Mar. 1993.

[12] *Guided-Wave Optoelectronics*, T. Tamir, Ed. New York: Springer-Verlag, 1990.

[13] Y. Yamada, A. Sugita, N. Moriwaki, I. Ogawa, and T. Hashimoto, "An application of a silica-on-terraced-silicon platform to hybrid Mach-Zehnder interferometric circuits consisting of silica-waveguides and $LiNbO_3$ phase-shifters," *IEEE Photon. Technol. Lett.*, vol. 6, pp. 822–824, July 1994.

[14] P. Yeh, "Electromagnetic propagation in birefringent layered media," *J. Opt. Soc. Amer.*, vol. 69, pp. 742–756, May 1979.

[15] J. S. Bagby, D. P. Nyquist, and B. C. Drachman, "Integral formulation for analysis of integrated waveguides," *IEEE Trans. Microwave Theory Technol.*, vol. MTT-33, pp. 906–915, Oct. 1985.

[16] E. W. Kolk, N. H. Baken, and H. Blok, "Domain integral equation analysis of integrated optical channel and ridge waveguides in stratified media," *IEEE Trans. Microwave Theory Technol.*, vol. 38, pp. 78–85, Jan. 1990.

[17] N. H. G. Baken, M. B. J. Diemeer, A. M. Van Splunter, and H. Blok, "Computational modeling of diffused channel waveguides using a domain integral equation," *J. Lightwave Technol.*, vol. 8, pp. 576–585, Apr. 1990.

[18] P. G. Cottis and N. K. Uzunoglu, "Integral-equation approach for the analysis of anisotropic channel waveguides," *J. Opt. Soc. Amer. A*, vol. 8, pp. 608–614, Apr. 1991.

[19] H. J. M. Bastiaansen, N. H. G. Baken, and H. Blok, "Domain-integral equation analysis of channel waveguides in anisotropic multi-layered media," *IEEE Trans. Microwave Theory Technol.*, vol. 40, pp. 1918–1926, Oct. 1992.

[20] J. S. Bagby, "Integral equation description of integrated dielectric waveguides," Ph.D. dissertation, Michigan State Univ., 1984.

[21] J. M. Grimm, "Non-bound contributions to the propagation-mode spectrum of open-boundary waveguides," Ph.D. dissertation, Michigan State Univ., 1992.

[22] G. W. Hanson, "Integral equation formulation for inhomogeneous anisotropic media Green's Dyad with application to microstrip transmission line propagation and leakage," *IEEE Trans. Microwave Theory Technol.*, vol. 43, pp. 1359–1363, June 1995.

[23] J. S. Bagby and D. P. Nyquist, "Dyadic Green's functions for integrated electronic and optical circuits," *IEEE Trans. Microwave Theory Technol.*, vol. MTT-35, pp. 206–210, Feb. 1987.

[24] R. F. Harrington, *Field Computation by Moment Methods*. New York: Macmillan, 1968.

[25] B. Ray, "Integral equation analysis of multilayered anisotropic dielectric waveguides with application to ARROW structures," M.S.E.E. thesis, Univ. Wisconsin—Milwaukee, 1994.

[26] D. Marcuse, *Theory of Dielectric Optical Waveguides*. New York: Academic, 1991, 2nd ed.

[27] K. Matsubara and H. Yajima, "Analysis of Y-branching optical circulator using magnetooptic medium as a substrate," *J. Lightwave Technol.*, vol. 9, pp. 1061–1067, Sept. 1991.

[28] A. Knoesen, T. K. Gaylord, and M. G. Moharam, "Hybrid guided modes in uniaxial dielectric planar waveguides," *J. Lightwave Technol.*, vol. 6, pp. 1083–1103, June 1988.

Bishwabandhu Ray, photograph and biography not available at the time of publication.

George W. Hanson was born in Glen Ridge, NJ, in 1963. He received the B.S.E.E. degree from Lehigh University, Bethlehem, PA, the M.S.E.E. degree from Southern Methodist University, Dallas, TX, and the Ph.D. degree from Michigan State University, East Lansing in 1986, 1988, and 1991, respectively.

From 1986 to 1988 he was a development engineer with General Dynamics in Fort Worth, TX, where he worked on radar simulators. From 1988 to 1991 he was a research and teaching assistant in the Department of Electrical Engineering at Michigan State University. He is currently Assistant Professor of Electrical Engineering at the University of Wisconsin in Milwaukee. His research interests include electromagnetic interactions in layered media, microstrip circuits, and microwave characterization of materials.

Dr. Hanson is a member of URSI Commission B, Sigma Xi and Eta Kappa Nu.